NUMERICAL SIMULATION OF THERMAL BLOOMING WITH LASER-INDUCED CONVECTION

BENJAMIN F. AKERS* AND JONAH A. REEGER†

Abstract. High energy laser propagation through an absorbing fluid is examined via numerical simulation. In contrast to typical thermal blooming studies, both the laser and fluid dynamics are simulated. The beam propagation is modeled with the paraxial equation. The fluid medium is modeled with the incompressible Navier-Stokes equations. The Boussinesq approximation is used to couple the temperature to density variations. In this context, the interplay between laser-induced convection and refraction is observed. The fluid is taken to be initially homogeneous and quiescent; scintillation due to background fluctuations is ignored.

Key words. Thermal Blooming, Fluid Dynamics, Laser, Numerical Simulation

1. Introduction

This article considers self-induced thermal effects on the propagation of continuous wave High Energy Lasers (HEL). The understanding of laser propagation is important in an ever increasing array of applications including targeting, wireless communication, energy transfer, remote sensing, cooling of Bose-Einstein condensate, measuring gravity-waves, and many more [1, 2, 3, 4]. For applications involving atmospheric propagation, continuous wave lasers exist with powers in the kilowatts [5], a number which is certain to increase with time. In laboratory settings, pulse lasers have been developed with powers reaching the staggering petawatts [6, 7]. In this paper, we develop a framework to numerically simulate the propagation of continuous wave HEL coupled with the fluid dynamics of the propagation medium, to study laser-induced convection and the resulting beam refraction.

It is unreasonable to directly simulate the dynamics of a fluid medium at both the scale of laser wavelengths and distance of beam propagation, as these typically differ by many orders of magnitude. The conventional approach is to use an envelope equation for the beam propagation, for example the paraxial equation [8, 9, 10], and a statistical description of the small scale fluctuations in the atmosphere, typically at a discrete sequence of phase-screens [11]. We will also use an envelope equation, but will include volumetric effects from the atmosphere by directly simulating the fluid flow.

Temperature fluctuations are the most common fluid quantity tracked in laser simulations. As the beam heats the fluid, changes in temperature result in changes to the refractive index. These changes in refractive index feed back upon the beam, resulting in an effect known as thermal blooming. Thermal blooming is a well documented phenomenon [10, 12, 13, 14], whose relevance to laser propagation in the atmosphere gains importance as lasers become more powerful. In this work, we consider a regime in which the laser heating is large enough to dominate any background temperature fluctuations or wind shear, but not so large as to cause molecular changes in the gas (i.e. to ionize or create a plasma as in [15]). Such a regime corresponds to rather high power densities when considered in atmospheric propagation scenarios, but relatively small power densities compared to the lasers often used in a laboratory or industrial setting. When such an approximation is valid depends not only

---

*Department of Mathematics and Statistics, Air Force Institute of Technology, WPAFB, OH, (Benjamin.Akers@afit.edu).

†Department of Mathematics, US Naval Academy, Annapolis, MD.

on the beam power and initial state of the fluid, but also on the laser frequency and absorbivity of the medium. In contrast to previous studies [16], we consider the problem on a convective timescale and include the action of buoyancy transverse to the beam (horizontal propagation). To date, all studies of thermal blooming consider the fluid *velocity* to be prescribed, either statistically or deterministically [12, 17, 18]. In contrast, we use a model wherein the fluid motion is a dynamic variable, solved for with the beam in a coupled system. The resulting model is numerically simulated to study the effect of laser-induced convection on thermal blooming.

The remainder of the paper is organized as follows. In section 2, we present the models used for simulation of the coupled beam and atmospheric dynamics. In section 3, we present the numerical methods and simulation results, including temperature and beam dynamics in time, the effect of varying Richardson number, and both spatial and temporal convergence studies. In section 4, we conclude and present future research areas.

2. Formulation In this section, we present the model equations used to study HEL propagation through the a dynamically heated fluid. These equations are the paraxial equation for the beam propagation, coupled with the incompressible Navier-Stokes equations for temperature and velocity fields of the fluid. The density is assumed to be near constant, with changes in density coupled to temperature fluctuations via the Bousssinesq approximation [19].

The physical setup for this problem has a separation of scales. The beam travels long distances (and varies slowly) in the propagation direction (z coordinate) but has a short pulse width in the transverse directions (x,y coordinates). In such circumstances, the paraxial equation can be derived as an approximation to Maxwell's equations [9], written below in scaled coordinates

$$\frac{\partial V}{\partial z} = \left(\frac{i}{2kn_0}\triangle_H - in_1k - \alpha\right)V, \tag{2.1}$$

where, n_0 is the mean refractive index, n_1 is a small correction to the refractive index, k is the wavenumber of the beam, α is loss due to absorption, and $\triangle_H$ is the Laplacian in the transverse xy-plane. This equation has been numerically simulated previously using, for example, the Fourier-split step method [20, 21, 22, 23, 24] or recently using finite volume method coupled with the Madelung transform in [25].

We make a classical choice, modelling the small corrections to the refractive index, n_1, in terms of ρ_1 the small density fluctuations from a mean density ρ_0, using the Gladstone-Dale relationship [26]

$$n_1 = (n_0 - 1)\frac{\rho_1}{\rho_0}. \tag{2.2}$$

Equation (2.2) is further simplified with the Boussinesq approximation for ideal gasses [19], which relates density fluctuations to temperature fluctuations as

$$\frac{\rho_1}{\rho_0} = \frac{T_1}{T_0},$$

in which T_0 is the reference temperature, from which T_1 is a small fluctuation. The result is a linear coupling between refractive index fluctuation and temperature fluctuation

$$n_1 = (n_0 - 1)\frac{T_1}{T_0}. \tag{2.3}$$

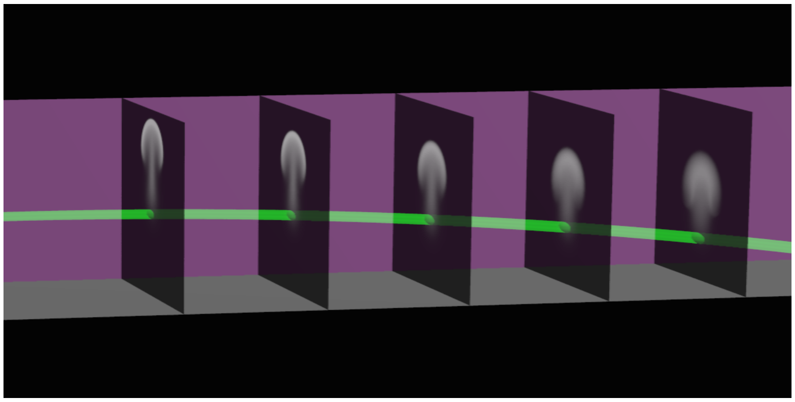

FIG. 2.1. *A schematic of the numerical setup is depicted. The fluid is evolved according to* (2.4) *on slices at a sampling of z values. Volumetric fluid quantities are obtained by interpolation between slices. The paraxial equation is then coupled to the volumetric temperature field via the refractive index. The beam deforms due to differences in refractive index (temperature-based), and both heats less further down the path, due to absorption, and heats at a different location, due to defraction.*

The temperature fluctuations are evolved in the incompressible Navier-Stokes equations, presented below in non-dimensional form.

$$u_t + (u\cdot\nabla)u = \nabla P + \frac{1}{\mathrm{Re}}\Delta u + \mathrm{Ri} T\vec{e_2} \tag{2.4a}$$

$$T_t + (u\cdot\nabla)T = \frac{1}{\mathrm{Pe}}\Delta T + \mathrm{St}|V|^2 \tag{2.4b}$$

$$\nabla\cdot u = 0 \tag{2.4c}$$

These equations have been non-dimensionalized using a beam width as the characteristic lengthscale L, a velocity scale U, a convective time scale $\tau = \frac{L}{U}$, a temperature scale T_0, a beam intensity scale of V_0, and a pressure scale of $P_0 = \rho_0 U^2$. The vector $\vec{e_2} = (0,1)$ is the unit vector in the vertical direction; this term is the manifestation of gravity in the Boussinesq regime. The variable T is the normalized temperature fluctuations $T = \frac{T_1}{T_0}$; in the numerical results section we report $T_1 = T_0 T$, so that our reported temperatures have the more intuitive units, degrees K. The fluid length and velocity scales are measured against g, ν and μ, the force due to gravity, the kinematic viscosity and thermal diffusivity respectively, typical choices in non-dimensional fluid simulations. The non-dimensional numbers which are introduced are the classic Reynolds (Re), Peclet (Pe), and Richardson (Ri), as well as the less common Stanton number (St) [27], all defined below,

$$\mathrm{Re} = \frac{UL}{\nu}, \qquad \mathrm{Pe} = \frac{UL}{\mu}, \qquad \mathrm{Ri} = \frac{gL}{U^2}, \qquad \mathrm{St} = \frac{\beta V_0^2 L}{U T_0}.$$

The last number tells the extent to which heat is concentrated, as it compares the rate of heat deposition by the beam to the rate of convective heat transfer in the fluid. The Stanton number is the one which grows with the energy of the laser (as well as with the absorbivity of the medium). We will consider flows with Stanton number $St = \frac{1}{30}$. This corresponds to a continuum of beam sizes, power densities and absorbivities. We prefer to consider the size of the Stanton number as a statement about the fluid flow, rather than the laser power; however, we recognize that there is a community of scientists for whom the laser power is of primary interest. As a concrete example of such a Stanton number, consider a laser at 1.045 μm, with a β for dry, clear air at $10^{-9}\frac{\text{K m}^2}{\text{J}}$, and a 1cm beam diameter at $300K$ with $g = 981\text{cm/sec}^2$. A Stanton number of $\frac{1}{30}$ and a Richardson number of 10^4 corresponds to a power density of $V_0^2 = 313\frac{\text{kW}}{\text{cm}^2}$. The value of the absorbivity, β, varies significantly based on the fluid medium, for example still at 1.045μm in air, it may be as high as $10^{-5}\frac{\text{K m}^2}{\text{J}}$ due to aerosol content, which results instead in a power density of $3\frac{\text{W}}{\text{cm}^2}$. The measurement and calculation of β, as well as total extinction coefficient, is non-trivial and an important current research field [24, 18, 28].

Although volumetric effects of the fluid are included in the beam equation, we do not solve (2.4) in three dimensions. The paraxial equation comes with an assumption of a separation of scales between the transverse, x and y, and the longitudinal, z, dependence of the beam amplitude, i.e. that if $V_x = O(\epsilon)$ then $V_z = O(\epsilon^2)$. In terms of this scale separation, the paraxial equation approximates Maxwell's equations to $O(\epsilon^2)$, and neglects higher order terms. To the same order of accuracy, the fluid flow is two dimensional (in x and y) and has no flow in the longitudinal coordinate $\mathbf{u} = (u_1, u_2, 0)$.

This study neglects the effect of scintillation due to small scale background fluctuations in the fluid medium. Scintillation often dominates the dynamics of laser propagation. For initially quiescent flows, or those where the energy transfer (measured by the Stanton number) are large, the thermal effects can dominate those of scintillation. An asymptotic study of the interplay between small turbulent fluctuations and large laser induced-convection is being pursued separately.

Our system is an example of a wave optics model, including a key novel feature relative to historical models. Early wave optics efforts included simulation of temperature dynamics, both in static fluids and prescribed fluid velocities, e.g. sidewinds and beam slewing [29, 26, 14, 30]. It is well known that, for low power or long propagation distance, even small turbulent fluctuations play an important role in beam dynamics. Modern models for these turbulent fluctuations are statistical, using prescribed realizations of fluid quantities[18, 31]. The fundamental difference between these wave optics models and the system in work is that rather than prescribing the fluid *velocities*, we solve for them as dynamic variables; the velocity is an unknown in our system, rather than a parameter. Laser propagation, including the effects of thermal blooming, are also often modeled with scaling laws [32, 33]. Scaling laws can be thought of an approximation the the results of a wave optics simulation, and thus the results of this work could be used in the future for the development of a scaling law including the effect of convective thermal blooming.

3. Numerical Results

To simulate the fluid equations, we solve (2.4) on transverse two-dimensional slices at a discrete series of locations, then interpolate between these slices. The resulting volumetric fluid quantities are used to determine the refractive index for the entire path of the beam in the paraxial equation. The resulting system has a quasi-two-dimensional cost for the fluid simulations, but still includes volumetric effects in the beam propagation. The quasi-two-dimensionality of the fluid system is a direct consequence of the paraxial scaling of the beam, as discussed earlier. A

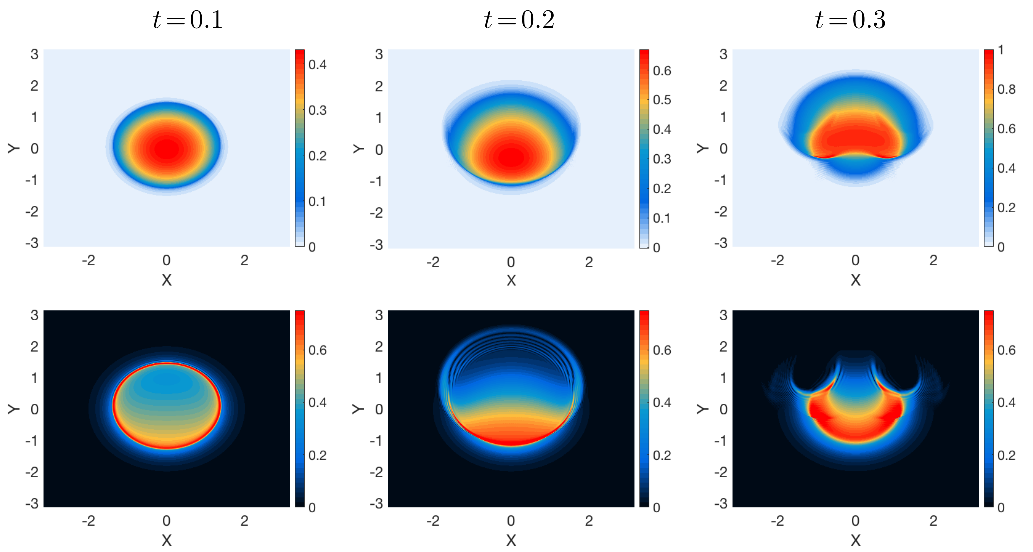

FIG. 3.1. *The temperature fluctuations T (top) and the intensity field $|V|$ (bottom) are depicted with laser-induced convection, results of simulations of equations* (2.1) *and* (2.4). *The simulations are at a distance of $z=800$, at a sampling of times, from left to right $t=0.1$, 0.2 and 0.3. The temperature fluctuations are reported in dimensional units, degrees Kelvin. For these simulations* $\eta_0=1.0003, T_0=300K, k=10^5, \beta=10^{-5}, St=\frac{1}{3}\times 10^{-1}, Ri=5\times 10^4, Re=10^3, Pe=10^3$.

diagram of the numerical setup is in figure 2.1, wherein two-dimensional slices of fluid are depicted, with a beam propagating in the transverse direction. These slices represent the locations where the fluid is evolved; between the slices fluid quantities are interpolated. The numerical methods for the evolution of this system, including discretization, convergence, and time solvers, are discussed in detail at the conclusion of this section.

We simulated the paired equations (2.1) and (2.4) in a regime where buoyancy plays a dominant role in the fluid flow, $Ri\approx 10^4$, with quiescent initial conditions, so that the beam heating drives any fluid motion. The choice of $St=\frac{1}{30}$ models a moderately large rate of energy deposition by the laser relative to the fluid's rate of thermal transport. The beam profile at the aperture, $z=0$, is held temporally fixed as a gaussian with constant phase,

$$V(x,y,0,t)=\exp\left(-(x^2+y^2)\right).$$

Both the fluid and laser equations are solved in the domain $(x,y)\in[-2\pi,2\pi)\times[-2\pi,2\pi)$ (although our figures typically report subsets of this domain). The temporal dynamics of one such simulation in this parameter regime are depicted in Figure 3.1.

An example of the temperature dynamics are in depicted in the top row of figure 3.1. Initially, for small heating, the beam has small refractive effects, and the temperature distribution is nearly radially symmetric (top left panel of figure 3.1). Radially symmetric temperature dynamics are typical of historical thermal blooming studies in which fluid velocities are neglected [14]. As time progresses, the warmer fluid rises and the beam deforms due the resulting asymmetry in the refractive index (center top panel of figure 3.1). At longer times, the heat rises convectively, leading to an increasingly mushroom shaped temperature distribution (top right panel of figure 3.1

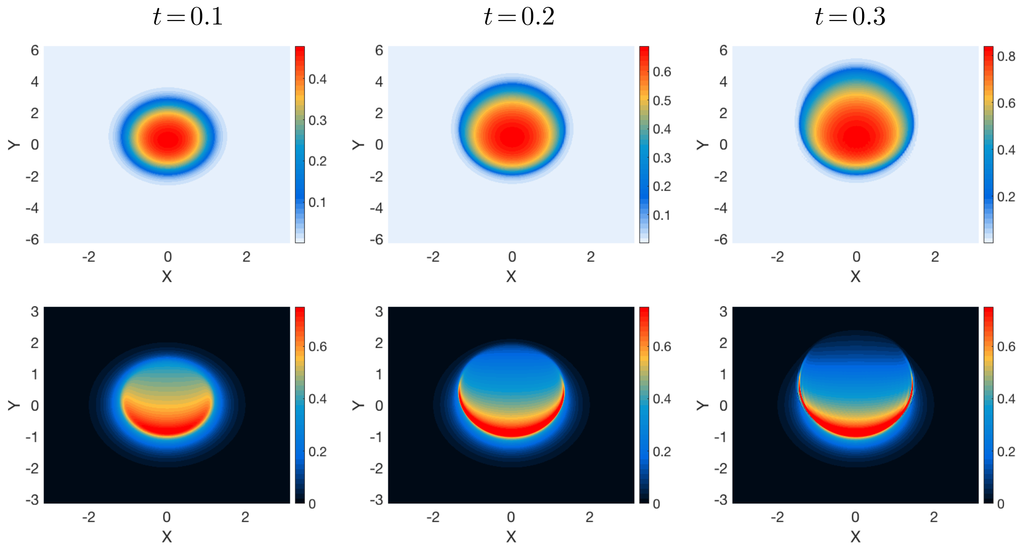

FIG. 3.2. *The temperature fluctuations T (top) and the intensity field $|V|$ (bottom) are depicted with a uniform cross wind, results of simulations of* (2.1) *and*(2.4) *but with prescribed vertical cross wind* $\mathbf{u}=(0,10)$. *The simulations are at a distance of* $z=800$, *at a sampling of times, from left to right* $t=0.1$, 0.2 *and* 0.3. *The temperature fluctuations are reported in dimensional units, degrees Kelvin. For these simulations* $\eta_0=1.0003, T_0=300K, k=10^5, \beta=10^{-5}, St=\frac{1}{3}\times 10^{-1}, Ri=5\times 10^4, Re=10^3, Pe=10^3$.

and the bottom right panel of figure 3.3).

As the temperature evolves so does the intensity of the beam. Asymmetric temperature fields cause the beam to deform asymmetrically (as has been observed many times in thermal blooming studies with specified wind [13, 25, 29, 30]), forming a crescent shape in the downwind direction. In contrast to a uniform wind, the velocity profile here varies on the scale of the beam spot size, resulting in a deformed crescent (bottom right panel of figure 3.1). The signature of the temperature field is evident in these deformations: the rounded holes at the tips of the crescent in the bottom right panel of figure 3.1, and the pinched corners of the crescent in the top right panel of figure 3.3 .

Asymmetric thermal blooming is commonly studied with a prescribed cross wind. To illustrate the qualitative differences between this experiment and laser-induced convection, we have included simulations of with a fixed uniform vertical cross wind of $\mathbf{u}=(0,10)$. No uniform cross wind can exactly correspond to the non-uniform and circulating currents induced by the laser heating. We choose the magnitude of the wind so that the shape and location of the beam spot was comparable on the time scale of our simulations. The results of these simulations are in figure 3.2. Notable differences are the earlier onset of the crescent shape (bottom left panel of figure 3.2), due to the fact the the cross wind instantly reaches at its maximum intensity; in the convective experiment the magnitude of the velocity field increases with time. Also, with a uniform cross wind the tips of the crescent become increasingly pointed in time; in the convective experiment stagnation zones occur in the vicinity of the tips of the crescent, creating more structure (the bottom right panel of figure 3.1).

In the equation (2.4), the time units are $\tau=\frac{L}{U}$, so the $Ri=\frac{g\tau^2}{L}$ can be thought

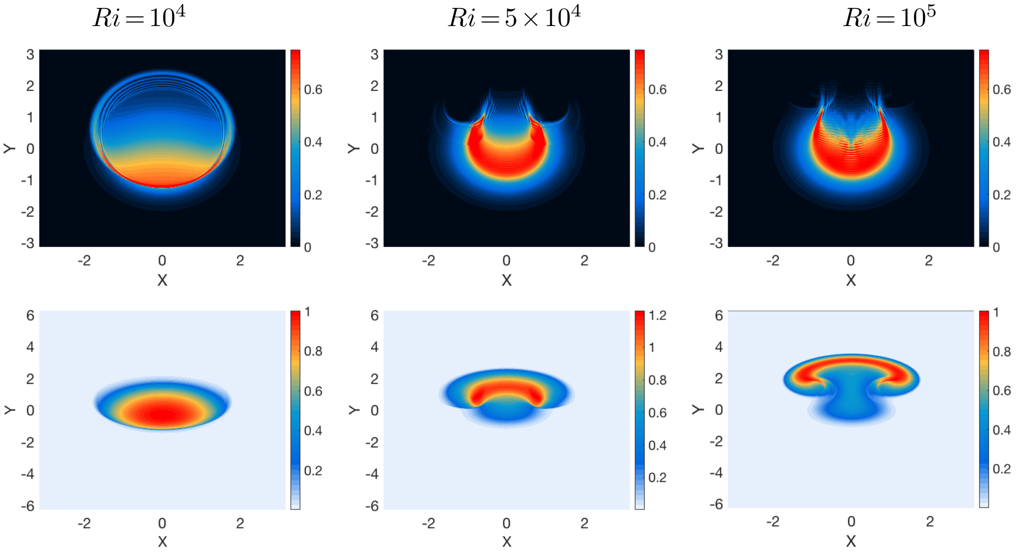

FIG. 3.3. *Top Row: Beam intensities at* $z = 800$*,* $t = 0.35$*, from left to right with* $Ri = 10^4$*,* $Ri = 5\times 10^4$ *and* $Ri = 10^5$*. Bottom Row: Corresponding temperature fluctuations from* $T_0 = 300K$*, reported in degrees, again reported at* $z = 800$*. All other parameters are the same as in Figure 3.1.*

of as measuring how long the experiment is observed, as compared to the natural gravitational timescale. We consider large Ri, long times relative to this gravitational timescale, with $Ri \in [10^4, 10^5]$. The effects of varying Richardson number with fixed Stanton number are portrayed in figure 3.3. As one should expect, larger Richardson number results in larger convection. From left to right the temperature fields in the bottom row of Figure 3.3 have more time to rise, resulting in increasingly mushroom shaped temperature fields. The corresponding beams spots become increasingly crescent shaped (top row of Figure 3.3).

The numerical methods used here utilize Fourier-collocation to approximate transverse, x and y, spatial derivatives and the sixth order Runge-Kutta of Luther [34] for evolution variables. In the paraxial equation (2.1), longitudinal distance, z, is the evolution variable; in the fluid equations (2.4), t is the evolution variable. A time splitting-scheme is used, allowing alternating evolution of the paraxial and Boussinesq equations. This alternation is done within a second order predictor-corrector method, whose operation over one time-splitting interval Δt_s we now describe. Over one time interval, a fixed beam intensity from the previous time step, $V(x,y,z,t_n)$, is used as the forcing in the fluid time solver to generate a predicted temperature field halfway though the splitting interval, denonted $\tilde{T}(x,y,z,t_n + \Delta t_S/2)$. This predicted temperature field is then input to the paraxial equation to generate a beam intensity corresponding to the temporal midpoint of the splitting interval, $V(x,y,z,t_n + \Delta t_S/2)$. The fluid quantities are then evolved from t_n to $t_n + \Delta t_S$ using a temporally constant beam, which was sampled at the midpoint of the time interval. The final temperature field $T(x,y,z,t_n + \Delta t_S)$ is then passed to the paraxial equation to generate the intensity at the next time step $V(x,y,z,t_n + \Delta t_S)$. The resulting method is second order in Δt_S. A convergence study in this parameter was conducted; the convergence rate is depicted in center panel of Figure 3.4.

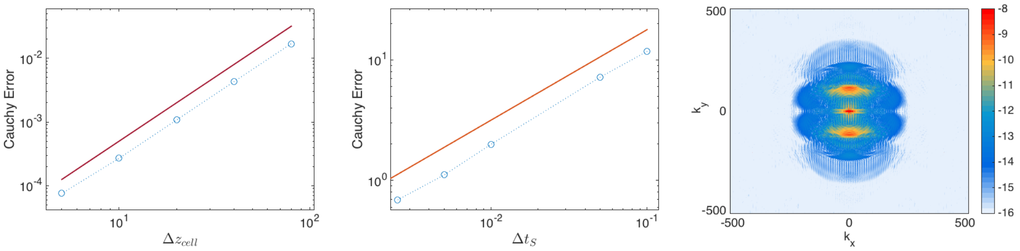

Fig. 3.4. *Numerical evidence of the convergence rate and spatial accuracy of the numerical method are presented. The left panel shows second order accuracy in the length of the cells over which the temperature field is interpolated Δz_{cell}. The center panel shows second order accuracy in the splitting time step between which the Boussinesq and Paraxial equations are alternately solved, Δt_S. The right panel shows the logarithm of the Fourier spectrum of the intensity at distance $z = 800$ at $t = 0.3$, which is localized in the frequency domain.*

There are a number of numerical parameters which contribute to errors of the numerical method, to varying degrees. Effectively all of these are truncation errors, from either the discretization of the evolution variables, from the splitting scheme, or from the interpolation of the temperature between fluid slices. The evolution of the Boussinesq equation uses a time step of $\Delta t = 0.5 \times 10^{-4}$, the paraxial equation with $\Delta z = 1$. Due to the highly accurate (sixth order Runge-Kutta) methods used for the evolution of the beam and fluid equations, these time-steps don't contribute significantly to the error. The truncation errors due to splitting are second order; the convergence in the time splitting parameter Δt_s is depicted in the center panel of Figure 3.4. The truncation errors due to interpolating the temperature between fluid slices, of cell length Δz_{cell}, was also carefully monitored. The temperature field was linearly interpolated over these cells, thus the convergence rate in cell length is theoretically second order. A convergence study in cell length, Δz_{cell} was conducted, verifying the theoretical prediction, and is depicted in the left panel of Figure 3.4.

4. Conclusions and future research

The interaction of beam-induced convection and refraction are studied via numerical simulation. The numerical procedure is developed specific to this application, allowing for observation of new phenomena. The influence of this convection creates qualitatively different beam spots from those observed in a slewed beam. Scintillation is neglected, however as the difference in the spot shape is qualitative, it can be expected to persist through the influence of small scintillation. The authors are currently pursuing an asymptotic study of the effects of small scintillation in this setting. The authors are also studying the effects of the alternate boundary conditions for the fluid solver, which currently limits the time of simulation, for example the free space boundary condition of Fornberg [35].

Disclaimer: This report was prepared as an account of work sponsored by an agency of the United States Government. Neither the United States Government nor any agency thereof, nor any of their employees, make any warranty, express or implied, or assumes any legal liability or responsibility for the accuracy, completeness, or usefulness of any information, apparatus, product, or process disclosed, or represents that its use would not infringe privately owned rights. Reference herein to any specific commercial product, process, or service by trade name, trademark, manufacturer, or otherwise does not necessarily constitute or imply its endorsement, recommendation, or favoring by the United States Government or any agency thereof. The views and opinions of authors expressed herein do not necessarily state or reflect those of the United States Government or any agency thereof.

Acknowledgements: Funding for this work was provided in part by the Office of Naval Research, as part of the APHSELs program as well as by the Air Force Office of Scientific Research under the program "Radial basis function for numerical simulation".

REFERENCES

[1] Larry C Andrews and Ronald L Phillips. *Laser beam propagation through random media*, volume 1. SPIE press Bellingham, WA, 2005.
[2] KN Liou, Szu-Cheng Ou, Yoshihide Takano, and Jeffrey Cetola. Remote sensing of three-dimensional cirrus clouds from satellites: application to continuous-wave laser atmospheric transmission and backscattering. *Applied optics*, 45(26):6849–6859, 2006.
[3] Richard J Bartell, Glen P Perram, Steven T Fiorino, Scott N Long, Marken J Houle, Christopher A Rice, Zachary P Manning, Dustin W Bunch, Matthew J Krizo, and Liesebet E Gravley. Methodology for comparing worldwide performance of diverse weight-constrained high energy laser systems. In *Proc. of SPIE Vol*, volume 5792, page 77, 2005.
[4] BP Abbott, R Abbott, R Adhikari, P Ajith, Bruce Allen, G Allen, RS Amin, SB Anderson, WG Anderson, MA Arain, et al. Ligo: the laser interferometer gravitational-wave observatory. *Reports on Progress in Physics*, 72(7):076901, 2009.
[5] DL Carroll. Overview of high energy lasers: past, present, and future. In *Proc. of 42nd AIAA Plasmadynamics and Laser Conf*, volume 3102, 2011.
[6] MD Perry, D Pennington, BC Stuart, G Tietbohl, JA Britten, C Brown, S Herman, B Golick, M Kartz, J Miller, et al. Petawatt laser pulses. *Optics Letters*, 24(3):160–162, 1999.
[7] Y Sentoku, TV Liseikina, T Zh Esirkepov, F Califano, NM Naumova, Y Ueshima, VA Vshivkov, Y Kato, K Mima, K Nishihara, et al. High density collimated beams of relativistic ions produced by petawatt laser pulses in plasmas. *Physical Review E*, 62(5):7271, 2000.
[8] Mark J Ablowitz. *Nonlinear Dispersive Waves: Asymptotic Analysis and Solitons*, volume 47. Cambridge University Press, 2011.
[9] Catherine Sulem and Pierre-Louis Sulem. *The nonlinear Schrödinger equation: self-focusing and wave collapse*, volume 139. Springer Science & Business Media, 2007.
[10] Daniel G Fouche, Charles Higgs, and C Frederick Pearson. Scaled atmospheric blooming experiments (sable). *The Lincoln Laboratory Journal*, 5(2):273–293, 1992.
[11] Rod Frehlich. Simulation of laser propagation in a turbulent atmosphere. *Applied Optics*, 39(3):393–397, 2000.
[12] David C Smith. High-power laser propagation: thermal blooming. *Proceedings of the IEEE*, 65(12):1679–1714, 1977.
[13] JA Fleck, JR Morris, and MD Feit. Time-dependent propagation of high energy laser beams through the atmosphere. *Applied Physics A: Materials Science & Processing*, 10(2):129–160, 1976.
[14] Frederick G Gebhardt. Twenty-five years of thermal blooming: an overview. In *OE/LASE'90, 14-19 Jan., Los Angeles, CA*, pages 2–25. International Society for Optics and Photonics, 1990.
[15] P Sprangle, E Esarey, and A Ting. Nonlinear theory of intense laser-plasma interactions. *Physical review letters*, 64(17):2011, 1990.
[16] Joseph R Penano, Phillip Sprangle, and Bahman Hafizi. Propagation of high energy laser beams through atmospheric stagnation zones. Technical report, NAVAL RESEARCH LAB WASHINGTON DC BEAM PHYSICS BRANCH, 2006.
[17] VA Banakh and AV Falits. Numerical simulation of propagation of laser beams formed by multielement apertures in a turbulent atmosphere under thermal blooming. *Atmospheric and Oceanic Optics*, 26(6):455–465, 2013.
[18] P Sprangle, JR Peñano, A Ting, and B Hafizi. Propagation of high-energy lasers in a maritime atmosphere. *Naval Research Labs*, 2004.
[19] David J Tritton. *Physical fluid dynamics.* Springer Science & Business Media, 2012.
[20] Jr. Fleck, J.A., J.R. Morris, and M.D. Feit. Time-dependent propagation of high energy laser beams through the atmosphere. *Applied physics*, 10(2):129–160, 1976.

[21] J. F. Schonfeld. The theory of compensated laser propagation through strong thermal blooming. *Lincoln Laboratory Journal*, 5:131–150, 1992.

[22] Rod Frehlich. Simulation of laser propagation in a turbulent atmosphere. *Appl. Opt.*, 39(3):393–397, Jan 2000.

[23] Stein Alec C. Baluyot and Nathaniel P. Hermosa Hermosa, II. Intensity profiles and propagation of optical beams with bored helical phase. *Opt. Express*, 17(18):16244–16254, Aug 2009.

[24] Phillip Sprangle, Joseph Peñano, and Bahman Hafizi. Optimum wavelength and power for efficient laser propagation in various atmospheric environments. *Journal of Directed Energy*, 2:71–95, 2006.

[25] J. Gustafsson, B.F. Akers, J.A. Reeger, and S.S. Sritharan. Atmospheric propagation of high energy lasers. *preprint*, 2017.

[26] Charles B Hogge. Propagation of high-energy laser beam in the atmosphere. Technical report, AIR FORCE WEAPONS LAB KIRTLAND AFB NM, 1974.

[27] Tuncer Cebeci and Peter Bradshaw. *Physical and computational aspects of convective heat transfer*. Springer Science & Business Media, 2012.

[28] Steven T Fiorino, Richard J Bartell, Matthew J Krizo, Gregory L Caylor, Kenneth P Moore, Thomas R Harris, and Salvatore J Cusumano. A first principles atmospheric propagation & characterization tool: the laser environmental effects definition and reference (leedr). In *Lasers and Applications in Science and Engineering*, pages 68780B–68780B. International Society for Optics and Photonics, 2008.

[29] Paul J Berger, Peter B Ulrich, Jeanne T Ulrich, and Frederick G Gebhardt. Transient thermal blooming of a slewed laser beam containing a region of stagnant absorber. *Applied optics*, 16(2):345–354, 1977.

[30] Le Wang and Wenbin Lin. The effect of wind directions on the thermal blooming of a laser beam propagating in the air. *Journal of Russian Laser Research*, 37(4):407–410, 2016.

[31] W Nelson, Phillip Sprangle, and CC Davis. Atmospheric propagation and combining of high-power lasers. *Applied optics*, 55(7):1757–1764, 2016.

[32] Noah R Van Zandt, Steven T Fiorino, and Kevin J Keefer. Enhanced, fast-running scaling law model of thermal blooming and turbulence effects on high energy laser propagation. *Optics express*, 21(12):14789–14798, 2013.

[33] VA Banakh and AV Falits. Efficiency of combined beam focusing under thermal blooming. *Atmospheric and Oceanic Optics*, 27(3):211–217, 2014.

[34] HA Luther. An explicit sixth-order runge-kutta formula. *Mathematics of Computation*, 22(102):434–436, 1968.

[35] Bengt Fornberg. Steady viscous flow past a sphere at high reynolds numbers. *Journal of Fluid Mechanics*, 190:471–489, 1988.